A Finite Element Model of Ultra-Sensitive Thin Film Calorimeters for the Study of Size-Dependent Thermodynamical Properties of Materials at the Nanoscale

R. Taillefer,[1] *P.Desjardins,*[1] *and F. Schiettekatte*[2]

[1] Département de Génie Physique, École Polytechnique de Montréal,
2 Département de physique, Université de Montréal
Groupe de recherche en physique et technologie des couches minces
P.O. Box 6079, Station Centre-Ville, Montréal, Québec, Canada, H3C 3A7

***Abstract* - We present a numerical model to study the dynamic behavior of ultra-sensitive thin film calorimeters. The finite element model includes direct coupling of thermal and electrical phenomena in order to evaluate the effects of materials, dimensions, and loading conditions on the physical behavior of the devices. The model is validated by simulating the melting of a thin metal film. Strategies to optimize the calorimeter design and operating conditions for experiments on advanced materials at the nanoscale are discussed.**

I. Introduction

Microelectromechanical systems (MEMS) are pervasive technologies, being increasingly used in, for example, automotive, communications, and biotechnological industries. It is anticipated that MEMS will revolutionize nearly every product category and will enable scientific breakthroughs in materials science, physics, chemistry, biology, and pharmaceuticals.

Predictive models allowing the simulation of MEMS behavior under a wide range of operating conditions are required for device design optimization. The well-known finite element analysis (FEA) modeling approach has been shown to yield accurate results in a variety of engineered structures. FEA models are now routinely used in the packaging industry [1-2]. Interest has grown in recent years for the development of coupled methods for simulating MEMS using thermal-electrical phenomena as the actuation principle [3-4]. Unfortunately, the models are in general very simplified in order to maintain the required computational effort at a reasonable level. This resulted, in most cases, in severe loss of accuracy.

In this article, we present a FEA model of thin film calorimeters used for the determination of size-dependent thermodynamical properties of ultrathin films and nanostructures [5-7]. Understanding size effects on materials properties such as melting point, specific heat, and heat of fusion is of critical importance for a variety of applications, for example in ULSI circuits as the half-pitch dimensions continue to decrease well below 100 nm. Furthermore, these ultra-sensitive calorimeters allow carrying out experiments designed to probe the mechanisms involved in the initial stages thin film formation or to study the properties of nanostructures.

To the best of our knowledge, we present the first fully-coupled (thermal-electrical) 3D FEA representation of a multilayered thin film device simulating a phase transition. Our model takes material non-linearities into account and can be solved in a reasonable time on a PC.

II. Constructing the FEA Model

Finite element modeling allows explicit coupling of physical phenomena, for example thermal and electrical in the present study.

Thermal behavior is examined by solving Fourier's law of heat conduction,

$$\rho c \cdot \frac{\partial T}{\partial t} - \nabla \circ \left(K \nabla T \right) = \dddot{q} \qquad (1)$$

where ρ, c and K are respectively the mass density, specific heat, and thermal conductivity of the materials of interest while $\partial T / \partial t$ is the heating rate. The right-hand term corresponds to the Joule heat generation rate per unit volume :

$$\dddot{q} = \frac{V(t) \cdot I(t)}{Vol} \qquad (2)$$

In Eq. (2), $V(t)$ and $I(t)$ are the real-time voltage drop and the current flowing in the calorimeter measured with a standard four-point probe method while Vol is the volume of material responsible for heat generation.

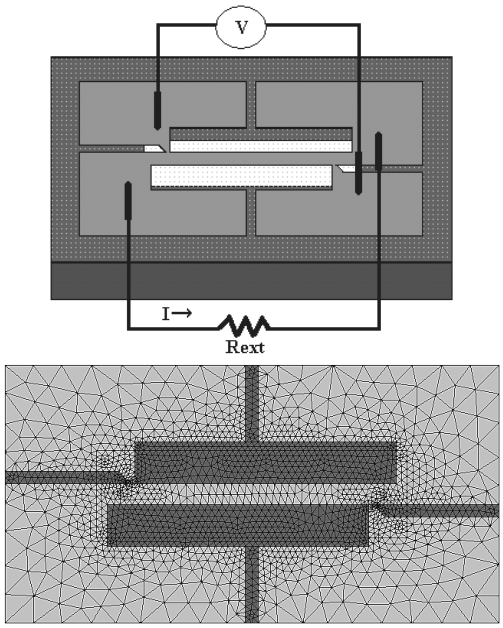

Fig. 1. Thin film calorimeter. (a) Solid model representation (not to scale). (b) Meshed FEA model.

The FEA model, created using ANSYS 7.0, consists of the calorimeter connected to an external resistor R_{ext} (Fig. 1a). The device is composed of a 100-nm-thick Si_3N_4 membrane covered with a patterned 50-nm-thick Ni metal strip. We consider a 25-µm-thick Si substrate. The external resistor serves to measure the current flowing through the calorimeter. It is maintained at constant temperature (no Joule heating) and is thermally isolated from the MEMS device. The external power supply is simulated as a constant voltage boundary condition between the positive terminal of R_{ext} and the ground node on the device. The boundary condition is applied as a ~10 ms pulse. We use temperature-dependent properties (ρ, c, K, and electrical resistivity ρ_e) for all materials. Correction factors [8] are applied to account for in-plane and out-of-plane size-dependent thermal conductivity for both Si_3N_4 and Ni. The electrical resistivity data are interpolated from $R(T)$ vs T calibration curves measured on microfabricated calorimeters with comparable dimensions.

Direct coupling between thermal and electrical domains is essential given the highly non-linear nature of thermal-electrical effects. We use shell-type elements for which coupling is established through a coupled matrix formulation between the two physical domains. It is important to mention that meshing of a true scale 3D model using traditional solid elements (bricks or tetrahedra) would result in an unreasonable number of elements (≈ 17 million), and thus computational effort, due to the enormous in-plane to thickness aspect ratio of approximately 230 000 for our device structures. We therefore use shell elements as an alternative representation of the device in the FEA domain. This type of element consists of a 2D mathematical representation of a 3D space and is therefore computationally more efficient than solid elements to model thin film materials.

Fig. 1b shows the meshed calorimeter. Although the structure is mathematically reduced to a two-dimensional problem through the use of shell elements, we have refined the mesh where large variations in thickness were observed in order to account for such discontinuities.

In the simulations presented here, we consider only heat flow occurring through conduction, neglecting radiation and convection losses. Radiation losses are expected to be minimal since our virtual experiments are limited to temperatures of 570 K and below. Since the calorimeter is operated in vacuum, convection losses are also considered negligible. Furthermore, Lai and al. [6] showed experimentally that a similar device operated under the same loading conditions consumed more than 94% of the power delivered.

III. Simulation of Phase Transition

We validate the FEA model by simulating the phase transformation (melting) of a 5-nm thick metal layer deposited on the calorimeter when considering enthalpy (Δ_m) vs T data as an input parameter (the materials properties of the metal layer are taken to be similar to those of Sn).

Transient thermal analyses were conducted on the circuit composed of the calorimeter loaded with the sample and the external resistor. We use time step increments of 10-µs (100-kHz sampling rate) combined with 3 different mesh densities to demonstrate the convergence of the numerical solution. The current in the external resistor and at the center metal strip of the calorimeter together with the voltage drop between the two metal inserts and the temperature distribution of the calorimeter are monitored continuously

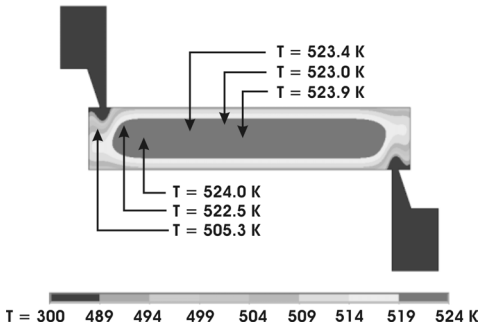

Figure 2: Temperature distribution of the nano-calorimeter after 7.12 ms of operation (not to scale).

during simulation. Based on these quantities, we compute the time-dependent resistance of the calorimeter as well as the power and energy delivered to the device. We then proceed to calculate the heating rate and the specific heat. In order to increase measurement sensitivity and to replicate the experimental use of the device, we carry out differential scanning calorimetry in which reference and loaded calorimeters are heated simultaneously [6].

Our simulation results indicate that T is very uniform over the whole device structure. Fig. 2 shows a typical temperature distribution plot, in this case after 7.12 ms of operation. Excluding the regions in the close vicinity of the inserts used for measuring $V(t)$ and a narrow band on the edges of the center strip, the temperature varies by less than 5 K over the calorimeter area.

The temperature vs time data for the reference and loaded calorimeters calculated from the electrical measurements on the inserts as described above are presented in Fig. 3. The slope for the reference calorimeter corresponds to a heating rate of 28 000 K s^{-1}, in good agreement with the value of 30 000 K s^{-1} measured experimentally on a calorimeter of similar dimensions operated in comparable conditions [5]. Fig. 3 clearly shows that the temperature T_s obtained from the device loaded with a metal sample lags behind the temperature T_r obtained from the unloaded calorimeter as expected from the higher thermal mass of the calorimeter covered with the Sn-like layer.

The heating rate of the loaded calorimeter presented in Fig. 4 exhibits a sharp decrease around the melting temperature T_m = 523.8 K. This value is in excellent agreement with the expected T_m value of 523.0±0.5 K given as a materials parameter. Temperature-dependent C_p values for the 5 nm-thick Sn-like layer are extracted from V(t) data by comparing loaded and reference calorimeters. The resulting curve, shown in Fig. 5, is almost identical to experimental data in Ref. [5]. It exhibits a maximum at 523.8 K as expected from the heating rate data in Fig. 4. The integrated area under the curve in Fig. 5 corresponds to a latent heat of fusion of 6.6 J g^{-1}, in very good agreement with the value of 6.5 J g^{-1} calculated based on the materials parameters. The heat surface density for this virtual experiment is ~240 mJ cm^{-2}, demonstrating the sensitivity of the device.

Based on simulations with different mesh densities, we attribute the wiggles on the trailing edge of the C_p peak in Fig. 5 to numerical noise. Increasing the mesh density near the inserts decreases the fluctuations in local temperature in those areas thus smoothening the C_p data profile. The integrated peak area, however, remains virtually unchanged. Furthermore, our detailed simulations indicate that there is little temperature variation on most of the length between the two

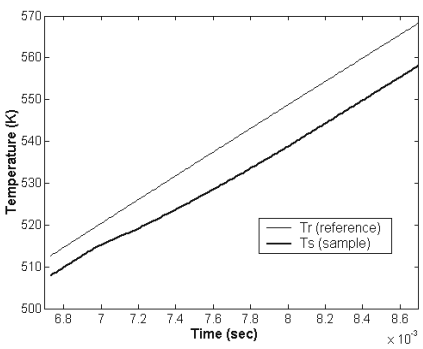

Fig. 3. Temperature vs time while heating reference and loaded calorimeters.

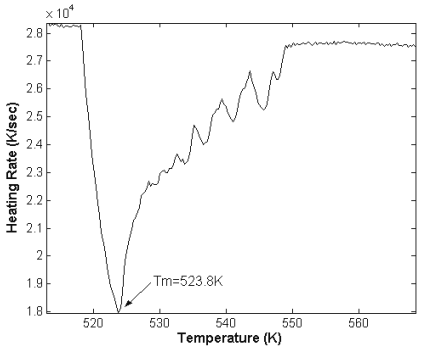

Fig. 4: Heating rate vs temperature during the melting of a 5-nm-thick metal film.

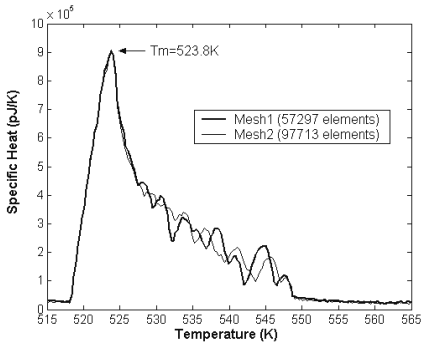

Fig. 5: Specific heat vs temperature during the melting of a 5-nm-thick metal film.

inserts, therefore justifying the calculation of *R(T)* through real-time *I-V* measurements.

The progression of the molten zone of the thin metal film is shown in Fig. 6. Melting occurs very uniformly over most of the calorimeter area as expected from the temperature distribution data in Fig. 2. It is worth nothing that the temperature difference between the front and the back side of the Si_3N_4 membrane is less than 0.05 K.

IV. Towards Design Optimization

One of our primary objectives in constructing a numerical model for the calorimeters is to enable optimization of device design and operating conditions for a variety of experiments on advanced materials. We have implemented a complete parametric model of the device that allows to vary loading conditions (supply value, initial conditions, etc.) and material combinations as well as overall device topology and dimensions. Since topological optimization requires the conception of different device layouts, we first focused on the following parameters: (i) layer thicknesses, (ii) materials properties, (iii) loading conditions, and (iv) sampling frequency. We have also parameterized extracted results such as voltage measurement, current, heating rate, specific heat, and temperature obtained. A variety of optimization tools and approaches including variable sweeping, random design generation, factorial generation of designs, which is comparable to corners simulation, enables to explore the design and operation space of the calorimeters. Furthermore, the parametric model allows to study the device sensitivity on the design variables.

Our initial optimization results clearly indicate that, contrary to common belief, decreasing the Si_3N_4 membrane thickness from 100 nm to, for example, 30 nm has virtually no effect on the temperature distribution except in the close vicinity of the inserts. In sharp contrast, reducing the metal strip thickness improves considerably the temperature uniformity since this layer is responsible for most of the heat dissipation.

V. Conclusion

In summary, we have presented a fully-coupled electrical-thermal model of an ultra-sensitive calorimeter. Our model reproduces extremely well the experimental behavior of the device, including the simulation of the melting thin metal layer. A parameterized model enabling device optimization has been discussed.

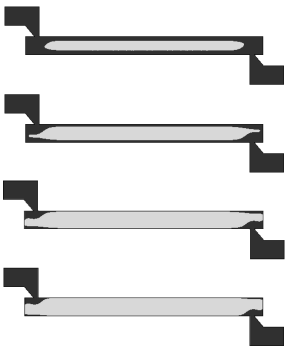

Fig. 6: Progression of the molten zone of the metal thin film during heating of the calorimeter. Black and light-gray regions correspond to solid and molten metal, respectively. From top to bottom, data after 7.25, 7.50, 7.75, and 8.00 ms.

Acknowledgements – The authors thank the Natural Sciences and Engineering Research Council of Canada (NSERC) and the Canada Research Chair program for financial support. Fruitful discussions with Les Allen are acknowledged.

References

[1] Li, R. S. and Larson, E., "An approach to thermal analysis of PCB with components having cyclic electrical loading", *ITHERM 2000. The 7th Intersociety Conf. on Thermal and Thermomechanical Phenomena in Electronic Systems,* Las Vegas, NV, USA, 2000.

[2] Xu, Y. L., Stout, R., and Billings, D., "Electronic package thermal response prediction to power surge", *ITHERM 2000. The 7th Intersociety Conference on Thermal and Thermomechanical Phenomena in Electronic Systems,* Las Vegas, NV, USA, 2000.

[3] Folkmer, B., Siber, A., Grobse Bley, W., Sandmaier, H., and Lang, W., Improved simulation for strongly coupled MEMS: resonant vacuum sensor optimization *Sensors and actuators A* 74, 190-2 (1999).

[4] Fabian, J. H., Scandella, L., et al., Finite element calculations and fabrication of cantilever sensors for nanoscale detection *Ultramicroscopy* 82, 69-77 (2000).

[5] Lai, S. L., Ramanath, G., and Allen, L. H., High-speed (10^4 °C/s) scanning microcalorimetry with monolayer sensitivity (J/m^2) *Appl. Phys. Lett.* 67, 1229-31 (1995).

[6] Lai, S. L., Ramanath, G., and Allen, L. H., Heat capacity measurements of Sn nanostructures using a thin-film differential scanning calorimeter with 0.2 nJ sensitivity *Appl. Phys. Lett.* 70, 43-45 (1997).

[7] Effremov, M. Yu., Schiettekatte, F., Zhang, M., Olson, E. A., Kwan, A. T., Berry, R. S., and Allen, L. H., Discrete Periodic Melting Point Observations for Nanostructure Ensembles *Phys. Rev. Lett.* 85, 3560 (2000).

[8] Flik, M. I. T. C. L., Size Effect on Thermal Conductivity of High-Tc Thin-Film Superconductors *Journal of Heat Transfer*, 112, 873-81 (1990).